THE ASTROPHYSICAL JOURNAL, 292:58–71, 1985 May 1

REDSHIFT EVOLUTION OF THE LYMAN-LINE–ABSORBING CLOUDS IN QUASAR SPECTRA

B. ATWOOD AND J. A. BALDWIN
Cerro Tololo Inter-American Observatory[1]
AND
R. F. CARSWELL[2, 3]
Institute of Astronomy, Cambridge
Received 1984 March 9; accepted 1984 November 12

ABSTRACT

The results of an analysis of the absorption lines measured on an echelle spectrum of the $z = 3.12$ quasar Q0420−388 are presented. The spectral resolution is sufficiently high (33 km s^{-1}) that most of the Lyman absorption lines are resolved, and so velocity dispersions and column densities have been obtained by profile fitting. Some selection effects make it difficult to be precise, but we find that the velocity dispersion $b[(2)^{1/2}\sigma_x]$ usually lies in the range 15–55 km s^{-1}, with a mean value of about 34 km s^{-1}. The H I column density number distribution is also uncertain, but may be approximated by a power law with exponent ≈ -2 for column densities $N(\text{H I}) > 10^{14}$ cm^{-2}.

By comparing the properties of the Lyman absorption systems at redshifts $z \approx 2$ to those at $z \approx 3$ we find that, apart from the numbers of detectable clouds, there is no evidence for redshift evolution in the distribution function for any measured quantity. Simple models in which a hot intergalactic medium pressure confined a comoving population of clouds are consistent with the available data if the clouds are nearly in thermal and ionization balance with the ionizing background flux from quasars. A significant population of low density adiabatically expanding clouds appears to be ruled out.

Subject headings: galaxies: intergalactic medium — quasars

I. INTRODUCTION

The statistical properties of the Lyman-line–absorbing clouds seen in quasar spectra have been extensively studied at intermediate resolution since Peterson (1978) noted that their numbers appear to be a steep function of the redshift. Further observational work by Sargent *et al.* (1980); Young, Sargent, and Boksenberg (1982); and Peterson (1983), among others, has confirmed and refined this result and provided us with a basis for models of the absorbing clouds. Their large numbers compared with systems which show heavy-element absorption lines, their apparent lack of heavy elements, and the absence of any clustering on scales we would expect from galaxies in a cluster combine to suggest that the Lyman-line–absorbing clouds are likely to be intergalactic (Sargent *et al.* 1980). The physical conditions in intergalactic clouds have been investigated further by Black (1981) and Ostriker and Ikeuchi (1983).

Recently, higher resolution spectroscopy has made it possible to measure H I column densities and velocity dispersions by fitting Voigt profiles to individual spectral features, and so to test some of the predictions, and assumptions, of different models for the Lyman-line–absorbing clouds. Chaffee *et al.* (1983) have drawn attention to one system in PHL 957 in which the velocity dispersion may be rather lower than one might expect if the cloud is typical of those in the intergalactic medium. Chaffee *et al.* (1984) have shown that the metal-to-hydrogen ratio in a cloud toward the QSO S5 0014+81 is less than 1/100 solar. Carswell *et al.* (1984) have obtained velocity dispersions and column densities for a number of clouds toward the $z = 2.14$ quasar Q1101−264, and have determined the distribution functions for these quantities at redshifts near $z = 2$.

In order to probe the properties of the clouds further, and particularly to look for any redshift-dependent properties, we have obtained a high resolution echelle spectrum of the redshift $z = 3.12$ quasar Q0420−388 (Smith 1976; Osmer and Smith 1976). Using this, we have been able to measure the parameters for a sample of Lyman-line systems at redshifts near $z = 3$. Comparison with the earlier work, especially that of Carswell *et al.* (1984), enables us to consider the statistical evolution of the clouds and compare it with some model predictions.

II. THE SPECTROSCOPIC DATA

Spectra of Q0420−388 were obtained using the SIT Vidicon detector (Atwood *et al.* 1979) attached to the echelle spectrograph at the Cassegrain focus of the Cerro Tololo Inter-American Observatory (CTIO) 4 m telescope. Observations were made using a 226 lines mm^{-1} cross-disperser (with first-order blaze at 8000 Å) in second order; the instrument was otherwise as described by Atwood, Baldwin, and Carswell (1982). A total of 11 hr of observing time was devoted to this object. The resolution obtained was 33 km s^{-1} (FWHM). Additional spectra, covering the wavelength range 3815–3950 Å at 19 km s^{-1} resolution (FWHM) were obtained using the Anglo-Australian Telescope (AAT), using the same instrument setup that has been described by Carswell *et al.* (1984). Some details of the observations are given in Table 1.

The combined spectrum is shown in Figure 1. For the wavelength region below 3950 Å only the AAT data were used. In the CTIO spectra between 3950 and 4150 Å the zero level is not well determined, probably because of some differential SIT fringing between object and sky channels which was not fully removed in the reduction procedure. The signal-to-noise ratio

[1] Cerro Tololo Inter-American Observatory is supported by the National Science Foundation under contract AST 78-27879.
[2] Visiting Astronomer, Cerro Tololo Inter-American Observatory.
[3] Radcliffe Fellow.

TABLE 1

OBSERVATIONS

Date (UT)	Wavelength Coverage	Integration Time (s)	Telescope	Comment
1981 Oct 30.21	echelle	10830	CTIO	
1981 Oct 31.19	echelle	14400	CTIO	
1981 Nov 1.19	echelle	14400	CTIO	
1982 Dec 4.68	3817–3950	6800	AAT	Thin cloud
1982 Dec 5.62	3817–3950	4800	AAT	some cloud

is low in this wavelength region, and so this zero-point uncertainty is of little consequence. The absorption-line wavelengths and equivalent widths were determined using the method described by Carswell *et al.* (1982). Heliocentric wavelengths and equivalent widths for these lines are given in Table 2.[4] Many of the lines are well resolved, so Voigt profiles, convolved with the instrumental profile, were fitted simultaneously to all available unblended lines of each ion for each cloud. These fits yield a redshift, velocity dispersion ($b = 2^{1/2}\sigma$), and column density for each cloud. Since with the SIT data we may make a reasonable estimate of the error term (see Atwood, Baldwin, and Carswell 1982), we have adopted a minimum χ^2 criterion for goodness of fit, and been able to estimate confidence limits for the derived quantities. Details of the procedure used, and some of its limitations, are discussed by Carswell *et al.* (1984).

A detailed point is that the failure to detect higher order Lyman lines at the redshift of a measured Lyα provides useful constraints on the velocity-dispersion and column-density parameters. Thus in determining these quantities at any redshift we have used all lines of the Lyman series which fall in our observed wavelength range and which are not badly blended, whether or not absorption features have been detected at their predicted positions. An indication of the Lyman lines used in each case is given in the comments column in Table 2. For example, $\alpha\beta\delta$ means that Lyα was detected, and Lyα, Lyβ, and Lyδ were used to determine the redshift, velocity dispersion, and column density for the system (though Lyβ and Lyδ were not necessarily detected). The Lyγ line in this example was not usable, presumably because it was found to be badly blended with some (Lyα?) line in another redshift system.

The equivalent widths of all lines given in Table 2 were measured using a smooth-continuum estimate, but the velocity dispersions and column densities were derived using a continuum modified to allow for the presence of weak lines in other systems. We chose to present the results in this way so that the equivalent widths are the directly observed quantities, and the velocity dispersions and column densities are the best estimates using all the data available. A consequence of this is that, for wavelengths below 4220 Å, the high-order Lyman lines from high-redshift systems often strongly affect the velocity dispersions and column densities given in the table. Thus in this region the quoted equivalent width will be consistent with the given velocity dispersion and column density in only a few cases, and the results depend to some extent on the redshift, velocity dispersion, and column density of some of the higher redshift clouds. At longer wavelengths the internal agreement is, as it should be, very good. Some small discrepancies occur because the parameter space is sampled over a finite grid to determine the best fit values, and also in a few cases where there is weak structure in the wings of a line which is not well fitted by a Voigt profile, but these are not significant.

For complex features we have used the minimum number of components which give a satisfactory fit to the blend. An unfortunate consequence of this is that the number of components found depends on the local signal-to-noise ratio (S/N) in the spectrum. Thus a feature which would be found to consist of two components at longer wavelengths in the Lyman forest may well be determined to arise from a single high velocity dispersion cloud if it occurred at shorter wavelengths where the S/N is poorer. Consequently, there appear to be fewer blended features at short wavelengths than long, and there is an apparent anticorrelation between the velocity dispersion and redshift in the Lyman line systems.

In some cases there is obvious blending of Lyβ by other lines (probably Lyα at lower redshift), and of Lyα by metal lines in known-redshift systems. We have omitted the obviously blended lines when fitting profiles, but it is not possible, in any particular case, to be sure that we do not have an undetected blend. Possible blending by higher order Lyman lines also affects our determination of the parameters for the Lyα clouds at redshifts $z_{abs} < 2.47$ ($\lambda_{obs} < 4220$ Å). Also, some Lyα lines may be missed because they underly a Lyβ (or other) line and are not significant features against the locally lower continuum. Note also that the S/N shortward of 4200 Å is sufficiently poor that only the strongest Lyβ and higher Lyman lines are detectable with certainty, so few are listed explicitly in Table 2.

In addition to the systems for which only Lyman lines have been detected, there are af few which also show heavy element lines. Smith *et al.* (1981) drew attention to an absorption system with very strong Lyman lines at $z_{abs} = 3.086$. The features they identify are clearly visible on our spectra, and, over the wavelength range where we have adequate S/N, the usual heavy-element lines are found. Analysis of the Si II line profiles reveals that the system must be at least triple, with redshifts $z_{abs} = 3.0857$, 3.0863, and 3.0882. The corresponding velocities relative to the lowest redshift system are 45 and 185 km s^{-1}, so it is not clear if a single galaxy or a cluster is responsible. The velocity separation with respect to the quasar is approximately 2500 km s^{-1}, so the galaxy or galaxies are unlikely to be in the same cluster as the quasar unless it is a particularly rich one.

There is also a group of C IV doublets in the red wing of the Lyα emission line at redshifts $z_{abs} = 2.2463$, 2.2619, and 2.2909. The corresponding Lyα absorption lines are present, but we have found no other lines in these systems. Each of the C IV doublets is well fitted by a single component, so there is no evidence for small-scale velocity structure. The velocities relative to the lowest redshift system are 1440 km s^{-1} and 4120 km s^{-1}. Such a velocity spread is rather large for systems which are

[4] The wavelengths given by Atwood, Baldwin, and Carswell (1983) are incorrect, and are 0.2 Å higher than the correct values used here. The error arose because of differences in the way wavelengths are assigned in the two computer programs that were used.

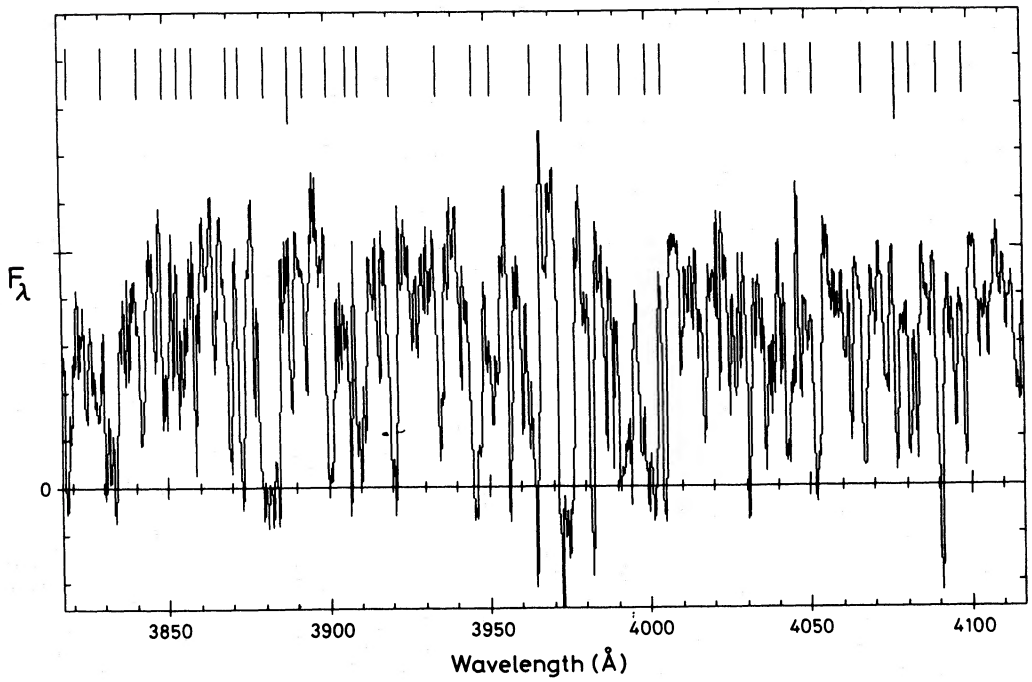

FIG. 1*a*

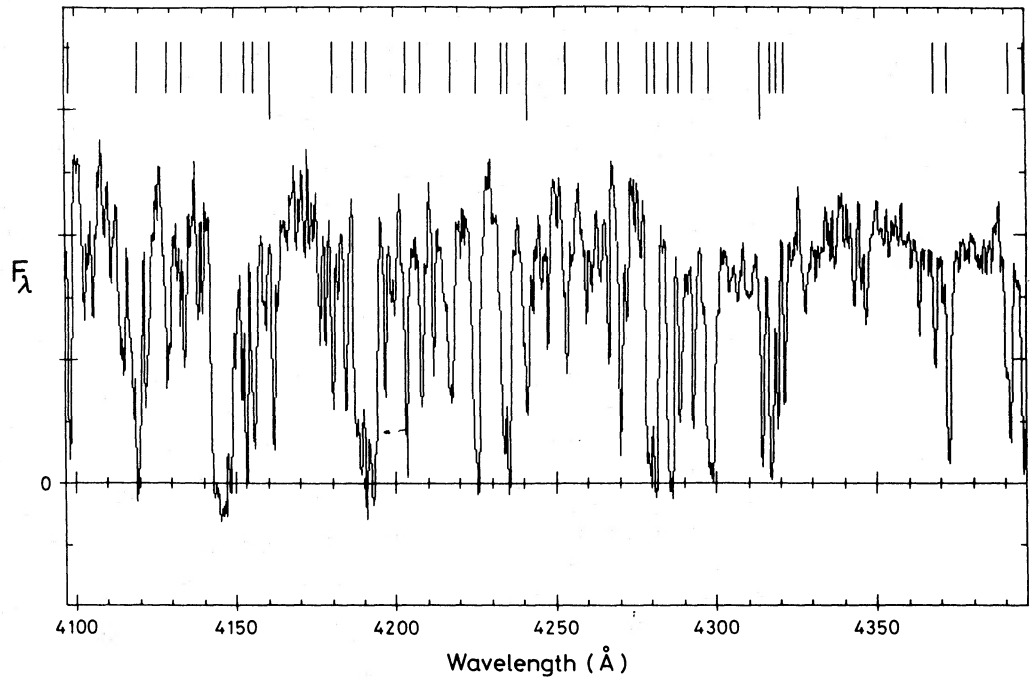

FIG. 1*b*

FIG. 1.—The spectrum of Q0420−388

in a cluster of galaxies, but since there are few other heavy-element line systems, it is tempting to suggest that the absorbing clouds might be associated in some way—e.g., in galaxies in a supercluster.

III. THE LYMAN LINE SYSTEMS

a) Observed Properties

There are 183 Lyman-line systems for which we have been able to determine redshifts and Lyα equivalent widths, and for 70 of these with redshifts $z_{abs} > 2.72$ we have been able to derive column densities and velocity-dispersion parameters by fitting at the positions of at least two lines in the Lyman series. Either the others are affected by gross confusion due to blending, or Lyα is the only Lyman line expected in the spectral region we have observed. Our S/N and resolution are together not always adequate to give an unambiguous result for a single

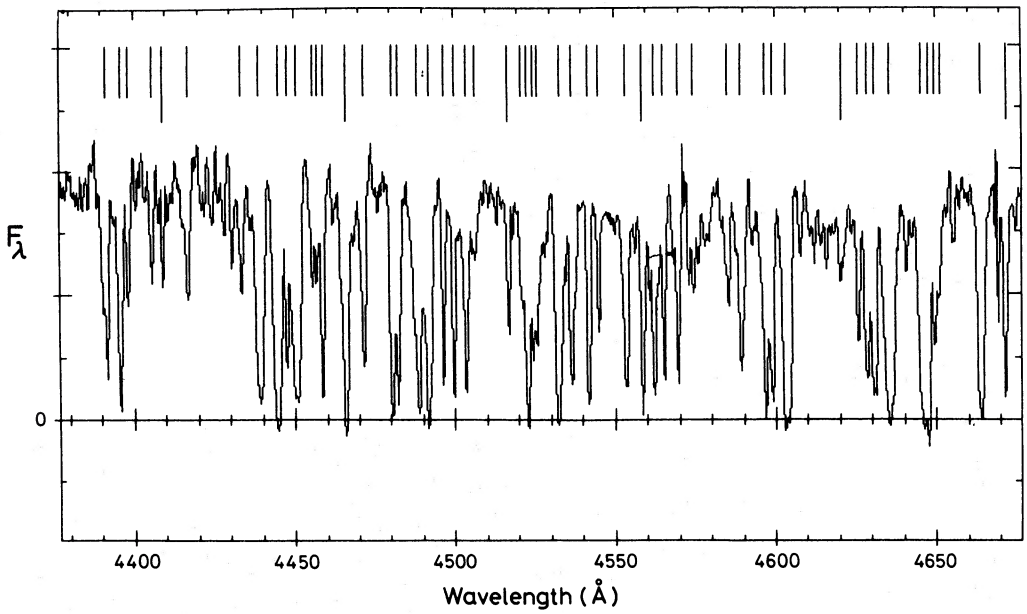

FIG. 1*c*

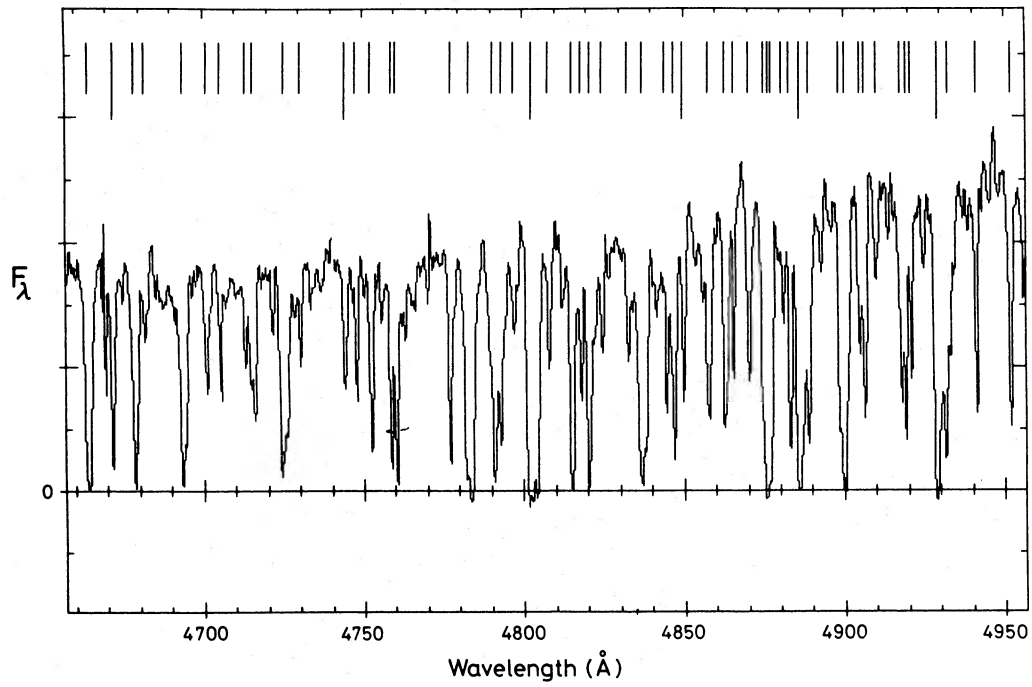

FIG. 1*d*

line, as is evident from the results presented in Table 2. Nor are the S/N and resolution always adequate to establish that apparently single features arise in only one cloud, or to unambiguously assign a number of clouds to a complex feature. What we have done is to establish parameters for the *minimum* number of clouds *consistent with the spectroscopic data*, and as a result we have to treat the distribution functions determined from these with some care.

To try to avoid such problems it is tempting to consider distribution functions derived from only the reliable determinations, but in some cases this could introduce a bias which could give misleading results. For example, a high-column-density cloud is less likely to have the Lyβ measurement badly affected by a lower redshift Lyα blend than is a low-column-density one, simply because the offending Lyα would have to be stronger to be noticeable against a strong Lyβ. On the other hand, inclusion of all lines which have been measured is undesirable because many have grossly unreliable velocity dispersion and column density determinations, especially where the S/N is low.

The equivalent widths of the Lyα lines are subject to few systematic effects, apart from a weak S/N–dependent uncertainty in the number of components in blends, especially at wavelengths less than 4200 Å ($z_{abs} < 2.45$) and contamination

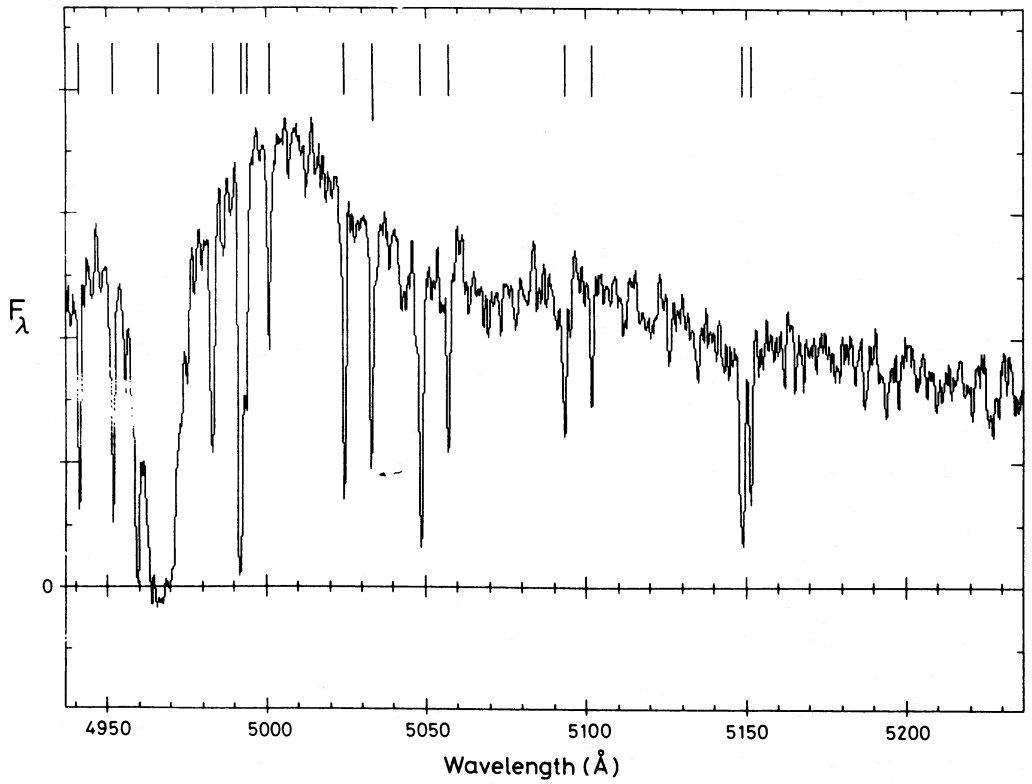

FIG. 1*e*

of the continuum by Lyβ, Lyγ, etc., from higher redshift systems for $z_{abs} < 2.47$. We therefore restrict consideration to systems for which $z_{abs} > 2.47$. In this range the rest equivalent width detection limit is about 0.15 Å, and so our list should be complete for systems with equivalent width $W > 0.2$ Å. For these we find that the form given by Sargent *et al.* (1980),

$$n(W, z) = A/W^* \exp(-W/W^*)dWdz ,$$

fits the equivalent width distribution quite well for $W^* = 0.26 \pm 0.03$ Å and $A = 284$ at $z = 2.8$. This result is in general disagreement with previous estimates based on spectra of different objects, obtained at differing resolutions, redshifts, and various detection limits (lower resolution by Sargent *et al.* 1980 yields $W^* = 0.36 \pm 0.02$; higher resolution by Carswell *et al.*, 1984 gives $W^* = 0.16 \pm 0.02$), and serves to highlight the suggestion made by the latter authors that the result obtained depends on the characteristics of the spectrum used. The differences may reflect no more than the ability to better resolve blends with improved resolution and S/N, but we have not investigated this point.

Combining the systems with $2.47 < z_{abs} < 3.08$ from Q0420−388 with those published by Carswell *et al.* (1984) for $z_{abs} \approx 2$ from Q1101−264 enables us to estimate the redshift dependence of the Lyα absorption-line density using material which is less subject to uncertainties from blending than the previous determinations (Peterson 1978; Sargent *et al.* 1980; Young, Sargent, and Boksenberg 1982; Peterson 1983). Unfortunately, there are few lines in the high-resolution sample and the redshift range is not very large, so the result is not very precise. For lines with rest equivalent widths greater than 0.2 Å, we find, for the number of clouds N_c per unit redshift z having an assumed form

$$\frac{dN_c}{dz} = A(1 + z)^\gamma ,$$

$\gamma = 1.7 \pm 1.0$. Given the error range, this is consistent with almost all the previous results (the Peterson 1978 determination was not to a uniform equivalent width limit, and so is not directly comparable). The value of the exponent γ depends to some extent on the chosen equivalent-width limit, but not by more than about ± 0.5 unless the limit is set so high that there are few lines in the sample. For example, for equivalent widths greater than 0.4 Å, $\gamma = 1.5 \pm 1.4$.

Because of biases affecting the determination of the H I column densities, their distribution function is less certain than that for the equivalent widths. If we restrict consideration to systems for which $N(\text{H I}) > 10^{14}$ cm^{-2} so that the effects of contamination of the higher order Lyman lines by lower redshift Lyα lines are more likely to be uniform, and require that at least two Lyman lines be unblended (so, necessarily, $z_{abs} > 2.72$), then, for an assumed probability distribution of the form

$$p(N) \propto N^{-\beta} dN ,$$

we find $\beta = 1.89 \pm 0.14$ for $10^{14} < N(\text{H I}) < 5 \times 10^{16}$ cm^{-2}. This is marginally steeper than, but consistent with, the value $\beta = 1.68 \pm 0.10$ found for redshift $z_{abs} \approx 2$ by Carswell *et al.* (1984).

The velocity-dispersion parameters b are generally distributed in the range $15 < b < 55$ km s^{-1}, with a peak at about 30–35 km s^{-1}. The mean value for the lines with $2.72 < z_{abs} < 3.12$ is $\langle b \rangle = 33.9 \pm 1.4$, somewhat higher than the value

TABLE 2

ABSORPTION LINES

n	λ_{air}	λ_{vac}	EW(A)	±	ID	z	±	b (km/s)	range	logN (/cm^2)	range	Comments
1	3819.38	3820.47	1.65	0.20	Lyα	2.14200	0.00033	1	<25	18.60	18.18–18.80	blend?
2	3830.21	3831.30	8.50	0.44	Lyϵ	3.08571				19.30	19.18–19.36	$\alpha\beta\gamma\delta\epsilon$)
					Lyϵ	3.08633				18.88	18.65–19.28	$\alpha\beta\gamma\delta\epsilon$) z from SiII
					Lyϵ	3.08824				19.40	19.32–19.49	$\alpha\beta\gamma\delta\epsilon$)
3	3841.47	3842.56	1.76	0.25	Lyγ	2.95132	0.00037	48	42–54	15.41	15.18–15.85	$\alpha\beta\gamma$
4	3849.15	3850.25	1.63	0.22	Lyα	2.16775	0.00028	38	13–95	13.80	13.36–14.86	noisy[a]
5	3854.15	3855.25	1.15	0.20	Lyα	2.17082	0.00011	8	<27	15.72	13.53–17.30	[a]
6	3858.62	3859.71	0.78	0.15	Lyα	2.17494	0.00010	13	6–31	15.88	13.88–17.43	[a]
7	3869.29	3870.39	1.72	0.23	Lyα	2.18394	0.00018	14	<63	17.48	14.00–18.04	[a]
8	3872.91	3874.00	2.12	0.22	Lyα	2.18681	0.00014	48	15–70	14.64	14.26–18.15	[a]
9	3881.22	3882.32	7.56	0.33	Lyδ	3.08571				19.30	19.18–19.36	$\alpha\beta\gamma\delta\epsilon$)
					Lyδ	3.08633				18.88	18.65–19.28	$\alpha\beta\gamma\delta\epsilon$) z from SiII
					Lyδ	3.08824				19.40	19.32–19.49	$\alpha\beta\gamma\delta\epsilon$)
10	3888.67	3889.78	0.83	0.15	Lyα	2.19976	0.00019	38	22–61	13.90	13.63–14.20	
11	3893.17	3894.27	0.64	0.16	Lyα	2.20350	0.00024	32	<80	13.70	13.34–17.49	
12	3900.66	3901.76	2.61	0.23	Lyα	2.20972	0.00032	71	37–99	14.65	14.32–17.08	[a]
13	3906.79	3907.89	1.28	0.25	Lyα	2.21466	0.00020	16	<40	14.86	13.57–17.59	[a]
14	3910.20	3911.30	2.99	0.25	Lyα	2.21684	0.00029	25	15–73	16.26	13.92–17.91	[a]
15	3920.07	3921.19	2.60	0.23	Lyβ	2.82252	0.00020	55	42–74	14.85	14.48–15.34	$\alpha\beta$
					Lyα	2.22607	0.00024	22	<54	14.52	13.75–17.89	
16	3934.79	3935.90	1.58	0.17	Lyβ	2.83709	0.00020	33	4–49	14.30	14.00–17.73	$\alpha\beta$
					Lyα	2.23747	0.00022	13	<55	15.70	13.43–17.65	
					Lyβ	2.83793	0.00010	27	20–36	14.53	14.28–14.93	$\alpha\beta$
17	3945.81	3946.93	3.90	0.27	Lyα	2.24626		24	9–31	18.32	16.78–19.59	z from CIV
					Lyα	2.24775	0.00040	53	24–80	14.00	13.71–14.51	[a]
18	3951.23	3952.35	2.14	0.50	Lyα	2.25092	0.00108	112	83–208	14.15	13.92–14.30	
19	3963.89	3965.01	3.50	0.60	Lyα	2.26187		43	<111	15.70	14.26–18.76	z from CIV
20	3973.86	3974.98	6.26	0.65	Lyγ	3.08571				19.30	19.18–19.36	$\alpha\beta\gamma\delta\epsilon$)
					Lyγ	3.08633				18.88	18.65–19.28	$\alpha\beta\gamma\delta\epsilon$) z from SiII
					Lyγ	3.08824				19.40	19.32–19.49	$\alpha\beta\gamma\delta\epsilon$)
21	3981.99	3983.12	1.98	0.42	Lyα	2.27644	0.00026	25	<73	16.11	14.11–18.34	
22	3992.00	3993.13	4.92	0.71	CIII 977	3.08571		10	<440	16.11	13.26–17.76	)
					CIII 977	3.08633		20	<630	16.70	12.75–18.26	) z from SiII
					CIII 977	3.08824		91	<770	14.00	13.18–18.28	)
					Lyα	2.28648	0.00037	20	<135	14.75	13.40–18.34	
23	3999.69	4000.82	5.81	0.67	Lyα	2.29086		53	<85	18.95	16.15–19.56	z from CIV
24	4004.61	4005.74	1.78	0.43	Lyα	2.29513	0.00026	25	<59	15.60	14.04–18.11	
25	4031.05	4032.19	1.71	0.38	Lyα	2.31686	0.00049	12	<33	17.60	13.59–18.28	[a]
26	4037.30	4038.44	2.10	0.46	Lyβ	2.93607	0.00014	40	32–47	15.00	14.72–15.28	$\alpha\beta\gamma$
27	4043.63	4044.77	2.34	0.42	NIII 989	3.08571		20	<150	16.51	14.26–18.97	z from SiII[a]
					SiII 989	3.08571	0.00010	8	4–21	14.00	13.28–15.60	
					SiII 989	3.08633	0.00013	32	22–45	13.71	13.58–13.91	
					SiII 989	3.08824	0.00007	4	2–21	15.79	13.36–16.08	
28	4051.76	4052.90	2.96	0.51	Lyβ	2.95132	0.00037	48	42–54	15.41	15.18–15.85	$\alpha\beta\gamma$
29	4067.07	4068.22	1.71	0.35	Lyα	2.34635	0.00055	42	<138	14.30	13.48–18.23	[a]
30	4077.34	4078.49	1.46	0.36	Lyα	2.35459	0.00025	18	<26	15.58	13.89–17.97	
31	4082.00	4083.15	2.39	0.42	Lyα	2.35789	0.00046	24	<165	14.23	13.04–18.04	[a]
					Lyα	2.35971	0.00024	9	<72	16.99	13.57–17.90	
32	4090.39	4091.55	2.52	0.36	Lyα	2.36572	0.00032	21	12–57	16.65	14.28–18.11	[a]
33	4098.05	4099.21	1.14	0.31	Lyα	2.37203	0.00027	24	<68	14.20	13.53–17.85	[a]
34	4119.70	4120.86	4.20	0.47	Lyα	2.38815	0.00060	100	34–800	14.00	13.59–14.83	[a]
					Lyα	2.38968	0.00043	43	<84	14.78	14.15–18.43	[a]
35	4128.73	4129.89	1.20	0.31	Lyα	2.39729	0.00044	75	34–135	13.91	13.61–14.23	

TABLE 2—*Continued*

n	λ_{air}	λ_{vac}	EW(A)	±	ID	z	±	b (km/s)	range	logN (/cm^2)	range	Comments
36	4133.68	4134.85	0.97	0.26	Lyβ	3.03160	0.00014	42	30–64	14.60	14.26–15.04	$\alpha\beta$
37	4145.93	4147.09	7.94	0.47	Lyα	2.41107	0.00023	80	67–150	18.08	15.40–19.11	
38	4153.23	4154.40	1.17	0.20	Lyα	2.41737	0.00015	17	<49	15.61	13.91–17.94	[a]
39	4155.69	4156.86	1.61	0.28	Lyα	2.41936	0.00025	57	25–98	14.20	13.94–15.89	
40	4161.12	4162.29	1.89	0.36	Lyα	2.42439	0.00019	10	<59	17.00	13.64–17.83	[a]
41	4180.43	4181.61	0.82	0.19	Lyα	2.43978	0.00021	30	<65	13.85	13.48–17.64	
42	4187.27	4188.45	0.84	0.15	Lyα	2.44548	0.00021	32	<61	14.00	13.62–17.78	
43	4191.15	4192.33	5.98	0.34	Lyα	2.44564	0.00026	42	<76	14.08	13.72–17.93	
					Lyβ	3.08571				19.30	19.18–19.36	$\alpha\beta\gamma\delta\epsilon$)
					Lyβ	3.08633				18.88	18.65–19.28	$\alpha\beta\gamma\delta\epsilon$) z from SiII
					Lyβ	3.08824				19.40	19.32–19.49	$\alpha\beta\gamma\delta\epsilon$)
					Lyα	2.45071	0.00023	29	<37	14.08	13.65–17.82	
44	4203.26	4204.44	1.29	0.24	Lyα	2.45861	0.00015	8	<50	17.48	13.88–17.88	
45	4208.23	4209.41	1.09	0.23	Lyα	2.46252	0.00021	42	17–91	13.94	13.65–14.97	
46	4217.17	4218.36	1.51	0.21	Lyα	2.46994	0.00031	80	54–123	14.15	13.92–14.30	
47	4225.09	4226.28	2.47	0.25	Lyα	2.47652	0.00015	57	20–84	14.70	14.32–18.18	
48	4233.39	4234.58	1.56	0.19	CII1036	3.08571		40	<86	14.30	14.04–18.08	)
					CII1036	3.08633		32	10–60	14.80	14.32–18.23	) z from SiII
49	4235.26	4236.45	1.45	0.18	Lyα	2.48477	0.00029	29	<59	14.43	13.86–18.04	
					CII1036	3.08824		20	<41	14.51	14.08–18.00	z from SiII
50	4240.93	4242.12	1.70	0.25	Lyα	2.48946	0.00034	80	51–136	14.04	13.88–14.20	
51	4253.11	4254.31	0.69	0.15	Lyα	2.49972	0.00015	1	<86	16.92	13.38–17.36	
52	4266.38	4267.58	0.46	0.11	Lyα	2.51049	0.00015	18	<38	13.70	13.36–17.15	
53	4270.12	4271.32	1.06	0.16	Lyα	2.51355	0.00011	30	<49	14.20	13.91–17.76	
54	4278.92	4280.12	2.04	0.14	Lyα	2.52088	0.00015	32	21–63	16.11	14.43–18.00	
55	4281.03	4282.24	1.88	0.15	Lyα	2.52254	0.00011	22	16–46	16.70	14.43–17.91	
56	4285.64	4286.84	2.43	0.18	Lyα	2.52633	0.00010	32	28–53	16.40	14.68–16.96	
57	4288.80	4290.01	1.32	0.17	Lyα	2.52885	0.00018	53	33–81	14.00	13.84–14.20	
58	4292.96	4294.17	1.08	0.17	Lyα	2.53227	0.00013	1	<57	17.46	13.77–17.74	
59	4298.14	4299.35	3.58	0.23	Lyα	2.53658	0.00012	100	58–130	14.60	14.46–14.88	
60	4314.03	4315.24	1.43	0.16	Lyα	2.54980	0.00011	40	18–59	14.15	13.97–15.26	
61	4316.96	4318.17	1.81	0.15	Lyα	2.55210	0.00010	40	<58	14.54	14.20–18.11	
62	4318.96	4320.18	0.83	0.11	Lyα	2.55373	0.00013	27	<43	13.94	13.71–17.54	
63	4321.13	4322.35	0.79	0.13	Lyα	2.55548	0.00012	27	<46	13.85	13.61–17.46	
64	4367.99	4369.22	0.61	0.11	Lyα	2.59417	0.00016	34	12–64	13.60	13.40–13.92	
65	4372.21	4373.44	1.77	0.16	Lyα	2.59767	0.00018	48	31–68	14.23	14.08–14.67	
66	4391.03	4392.26	1.58	0.14	Lyα	2.61240	0.00018	35	15–63	13.66	13.43–13.83	or CII 1334 z=2.29086
					Lyα	2.61347	0.00009	27	<44	14.08	13.85–17.68	
67	4395.63	4396.87	1.62	0.13	Lyα	2.61686	0.00009	45	29–57	14.28	14.11–15.00	
68	4398.16	4399.39	0.60	0.11	Lyα	2.61887	0.00016	32	14–54	13.60	13.41–13.81	
69	4405.49	4406.73	0.48	0.10	Lyα	2.62498	0.00018	32	11–53	13.48	13.23–13.67	
70	4408.99	4410.23	0.38	0.08	Lyα	2.62781	0.00013	16	<35	13.48	13.18–16.81	
71	4416.71	4417.95	0.68	0.12	Lyα	2.63417	0.00016	39	23–62	13.64	13.46–13.79	
72	4433.28	4434.53	0.64	0.12	Lyα	2.64782	0.00022	50	21–82	13.60	13.38–13.80	
73	4438.81	4440.06	2.84	0.17	Lyα	2.65251	0.00009	71	52–88	14.56	14.38–15.11	
74	4444.50	4445.74	3.05	0.14	Lyα	2.65706	0.00009	60	30–77	15.00	14.59–18.04	
75	4447.46	4448.71	1.04	0.10	Lyα	2.65948	0.00014	33	20–50	13.99	13.83–14.59	
76	4450.33	4451.58	2.86	0.14	Lyα	2.66184	0.00010	79	60–90	14.54	14.26–15.04	
77	4455.34	4456.59	0.49	0.10	Lyα	2.66601	0.00014	1	<58	16.43	13.15–16.80	
78	4456.75	4458.01	0.39	0.07	Lyα	2.66703	0.00020	30	<72	13.45	13.18–16.76	
79	4458.53	4459.78	1.14	0.11	Lyα	2.66858	0.00007	9	<39	17.26	13.94–17.63	
80	4465.57	4466.82	2.52	0.14	Lyα	2.67446	0.00009	67	40–79	14.45	14.34–14.60	
81	4471.13	4472.38	1.25	0.11	Lyα	2.67907	0.00009	45	30–57	14.00	13.89–14.18	
82	4480.30	4481.55	1.77	0.10	Lyα	2.68642	0.00008	22	16–36	15.70	14.45–17.34	
83	4482.19	4483.45	1.25	0.09	Lyα	2.68791	0.00009	42	26–58	14.20	14.04–14.52	

TABLE 2—*Continued*

n	λ_{air}	λ_{vac}	EW(A)	±	ID	z	±	b (km/s)	range	logN (/cm^2)	range	Comments
84	4488.10	4489.36	2.62	0.15	Lyα	2.69192	0.00023	55	18–92	13.67	13.43–13.83	
					Lyα	2.69326	0.00009	52	31–78	14.36	14.23–15.15	
85	4491.58	4492.84	2.40	0.13	Lyα	2.69585	0.00008	47	28–63	14.70	14.38–16.26	
86	4496.28	4497.54	0.95	0.10	Lyα	2.69960	0.00007	22	4–33	14.11	13.85–17.36	
87	4499.69	4500.95	1.26	0.13	Lyα	2.70231	0.00007	9	<32	17.15	13.95–17.57	
88	4503.34	4504.61	1.40	0.11	Lyα	2.70547	0.00009	43	28–56	14.08	13.96–14.36	
89	4506.01	4507.27	0.45	0.12	Lyα	2.70763	0.00035	55	30–115	13.40	13.11–13.60	
90	4516.65	4517.91	0.61	0.10	Lyα	2.71647	0.00010	1	<37	16.88	13.48–17.15	
91	4520.64	4521.91	0.47	0.08	Lyα	2.71987	0.00021	45	26–77	13.60	13.41–13.76	
92	4522.65	4523.92	2.07	0.11	Lyα	2.72134	0.00010	18	13–41	16.94	14.36–17.86	α
93	4524.47	4525.74	0.66	0.07	Lyα	2.72273	0.00021	42	18–94	13.86	13.66–14.11	α
94	4525.91	4527.17	0.97	0.11	Lyα	2.72392	0.00030	62	34–102	13.80	13.61–13.94	α
95	4532.59	4533.86	2.70	0.15	Lyα	2.72892	0.00009	32	22–45	14.34	14.08–14.75	αβ
					Lyα	2.72985	0.00011	32	21–44	14.45	14.15–14.93	αβ
96	4536.70	4537.97	1.50	0.12	Lyα	2.73274	0.00008	40	23–57	14.11	13.95–14.46	α
97	4541.74	4543.01	1.27	0.10	Lyα	2.73705	0.00007	18	13–32	15.71	14.20–17.18	α
98	4544.94	4546.22	0.49	0.08	Lyα	2.73968	0.00010	15	<30	13.70	13.41–16.99	α
99	4553.25	4554.53	1.57	0.12	Lyα	2.74657	0.00011	49	38–63	14.18	14.04–14.40	α
100	4558.52	4559.79	1.37	0.12	Lyα	2.75079	0.00007	30	22–40	14.34	14.11–14.68	αβ
101	4562.01	4563.29	1.78	0.14	Lyα	2.75257	0.00012	4	<24	14.40	13.04–16.56	α
					Lyα	2.75378	0.00008	32	22–47	14.26	14.04–14.70	αβ
102	4565.11	4566.39	0.89	0.10	Lyα	2.75629	0.00007	18	10–29	14.30	13.89–16.04	αβ
103	4569.57	4570.85	1.03	0.11	Lyα	2.75990	0.00009	29	19–41	14.04	13.85–14.36	αβ
104	4574.33	4575.62	0.43	0.09	Lyα	2.76385	0.00027	43	16–105	13.49	13.23–13.66	α
105	4585.03	4586.32	0.64	0.10	Lyα	2.77270	0.00021	44	29–69	13.57	13.38–13.73	α
106	4589.22	4590.50	1.54	0.14	Lyα	2.77615	0.00013	60	43–73	14.04	13.94–14.18	α
107	4596.52	4597.81	1.89	0.13	Lyα	2.78223	0.00009	53	40–71	14.28	14.15–14.54	α
108	4598.73	4600.02	1.44	0.11	Lyα	2.78391	0.00010	38	5–52	14.23	14.04–17.81	α
109	4603.33	4604.62	3.28	0.15	Lyα	2.78744	0.00040	50	15–65	14.77	14.38–18.26	α
					Lyα	2.78833	0.00022	40	18–54	14.57	14.20–17.45	α
110	4620.59	4621.88	0.61	0.12	Lyα	2.80177	0.00007	66	37–131	13.52	13.30–13.71	αβ
111	4625.70	4627.00	0.85	0.11	Lyα	2.80615	0.00011	36	23–50	13.80	13.65–13.97	αβ
112	4628.33	4629.63	1.45	0.11	Lyα	2.80841	0.00012	53	41–68	14.20	14.04–14.34	αβ
113	4630.60	4631.84	1.81	0.12	Lyα	2.80973	0.00011	9	<30	15.18	13.61–17.36	α
					Lyα	2.81044	0.00010	28	15–41	14.15	13.94–15.23	αβ
114	4635.28	4636.58	3.84	0.17	Lyα	2.81373	0.00025	57	46–72	14.64	14.41–14.95	αβ
					Lyα	2.81483	0.00037	60	33–82	14.18	14.00–14.69	α
115	4645.28	4646.58	2.17	0.13	Lyα	2.82252	0.00020	55	42–74	14.85	14.48–15.34	αβ
116	4647.37	4648.67	2.00	0.10	Lyα	2.82410	0.00009	28	23–38	14.51	14.26–14.85	αβ
117	4649.50	4650.81	0.89	0.09	Lyα	2.82559	0.00013	33	18–55	13.76	13.56–13.92	αβ
118	4651.00	4652.30	0.46	0.10	Lyα	2.82669	0.00024	50	23–87	13.60	13.36–13.76	αβ
119	4663.85	4665.16	2.45	0.16	Lyα	2.83709	0.00020	33	4–49	14.30	14.00–17.73	αβ
					Lyα	2.83793	0.00010	27	20–36	14.53	14.28–14.93	αβ
120	4671.43	4672.74	1.21	0.11	Lyα	2.84373	0.00008	24	18–34	14.38	14.04–14.78	αβ
121	4678.36	4679.67	1.93	0.13	Lyα	2.84955	0.00010	52	35–64	14.28	14.18–14.63	α
122	4681.57	4682.89	0.45	0.11	Lyα	2.85212	0.00031	45	6–82	13.34	13.04–13.56	α
123	4693.52	4694.83	2.39	0.15	Lyα	2.86171	0.00026	51	37–71	14.20	14.04–14.40	αβ
					Lyα	2.86253	0.00016	35	16–53	14.00	13.83–15.08	α
124	4701.17	4702.49	0.87	0.13	Lyα	2.86816	0.00020	47	26–74	13.70	13.52–13.83	αβ
125	4705.34	4706.65	0.57	0.11	Lyα	2.87170	0.00010	15	7–32	13.64	13.40–14.74	αβ
126	4713.12	4714.44	0.52	0.10	Lyα	2.87810	0.00019	29	7–69	13.48	13.26–14.08	α
127	4715.50	4716.82	1.40	0.13	Lyα	2.87934	0.00021	15	<44	13.46	13.18–16.86	αβ
					Lyα	2.88034	0.00012	37	26–55	13.87	13.73–14.04	αβ
128	4725.19	4726.52	2.73	0.15	Lyα	2.88718	0.00008	26	12–38	14.23	13.98–16.34	αβ
					Lyα	2.88791	0.00039	2	<99	16.60	13.08–17.34	α for b=10, logN=13.74
					Lyα	2.88870	0.00018	53	35–75	14.00	13.86–14.15	αβ

TABLE 2—*Continued*

n	λ_{air}	λ_{vac}	EW(A)	±	ID	z	±	b (km/s)	range	logN (/cm^2)	range	Comments
129	4730.45	4731.77	0.44	0.09	Lyα	2.89230	0.00018	25	<51	13.45	13.20–16.85	α
130	4744.30	4745.63	0.78	0.12	Lyα	2.90370	0.00018	41	25–61	13.71	13.53–13.85	αβ
131	4747.71	4749.03	0.73	0.12	Lyα	2.90669	0.00010	22	9–35	13.70	13.51–14.60	αβ
132	4752.37	4753.70	1.15	0.12	Lyα	2.91039	0.00008	30	19–43	14.11	13.89–14.77	αβ
133	4758.57	4759.91	1.11	0.11	Lyα	2.91548	0.00008	22	11–33	14.18	13.90–16.11	αβ
134	4760.36	4761.69	1.37	0.11	Lyα	2.91688	0.00009	32	22–44	14.28	14.04–14.93	αβ
135	4777.29	4778.62	1.29	0.14	Lyα	2.93078	0.00008	20	15–32	14.64	14.04–15.18	αγ
136	4783.14	4784.47	3.58	0.19	Lyα	2.93492	0.00020	42	26–60	14.26	14.08–14.61	αβ
					Lyα	2.93607	0.00014	40	32–47	15.00	14.72–15.28	αβγ
137	4790.47	4791.81	2.18	0.15	Lyα	2.94061	0.00030	42	12–95	13.38	13.08–13.63	α
					Lyα	2.94205	0.00010	43	29–68	14.32	14.15–14.96	αβ
138	4793.07	4794.41	1.34	0.12	Lyα	2.94360	0.00014	55	37–87	14.04	13.91–14.18	α
139	4796.87	4798.22	0.52	0.13	Lyα	2.94692	0.00041	48	12–100	13.40	13.11–13.62	α
140	4802.73	4804.08	4.39	0.17	Lyα	2.95132	0.00037	48	42–54	15.41	15.18–15.85	αβγ
					Lyα	2.95270	0.00022	40	34–53	14.65	14.36–14.86	αβγ
141	4807.67	4809.01	0.55	0.12	Lyα	2.95592	0.00015	26	7–49	13.52	13.30–14.18	αβ
142	4814.90	4816.24	1.88	0.13	Lyα	2.96177	0.00009	33	27–45	14.75	14.34–15.11	αγ
143	4817.70	4819.04	0.69	0.10	Lyα	2.96416	0.00014	22	9–39	13.70	13.49–14.30	αβ
144	4820.54	4821.89	2.20	0.15	Lyα	2.96611	0.00009	35	27–52	14.58	14.20–14.94	αγ
					Lyα	2.96767	0.00040	40	14–96	13.40	13.11–13.63	αγ
145	4824.21	4825.56	0.56	0.11	Lyα	2.96954	0.00019	35	17–62	13.52	13.28–13.68	αβγ
146	4832.51	4833.86	0.64	0.12	Lyα	2.97625	0.00022	38	18–74	13.56	13.34–13.72	αβγ
147	4836.79	4838.14	3.18	0.16	Lyα	2.97942	0.00021	57	33–76	14.40	14.23–15.00	α
					Lyα	2.98067		38	21–51	14.11	13.54–14.72	αβγ
148	4844.16	4845.51	0.85	0.12	Lyα	2.98609	0.00010	21	10–40	13.77	13.57–14.28	αβγ
149	4846.61	4847.97	1.49	0.13	Lyα	2.98800	0.00009	21	17–29	14.78	14.32–15.18	αβγ
150	4849.69	4851.04	0.76	0.11	Lyα	2.99045	0.00012	27	13–40	13.75	13.57–14.15	αβ
151	4857.63	4858.99	1.35	0.09	Lyα	2.99686	0.00012	48	34–61	14.00	13.88–14.18	αγ
152	4862.85	4864.21	1.39	0.12	SiII1190	3.08571		8	4–21	14.00	13.28–15.60	
					SiII1190	3.08633		32	22–45	13.71	13.58–13.91	
153	4865.36	4866.72	0.45	0.07	SiII1190	3.08824	0.00007	4	2–21	15.79	13.36–16.08	
154	4870.24	4871.60	0.81	0.11	Lyα	3.00734	0.00013	30	18–45	13.67	13.51–13.84	αβγ
155	4874.70	4876.06	1.52	0.10	SiII1193	3.08571		8	4–21	14.00	13.28–15.60	
					SiII1193	3.08633		32	22–45	13.71	13.58–13.91	
156	4876.00	4877.36	0.93	0.06	Lyα	3.01227	0.00020	48	38–59	14.70	14.41–15.11	αβ
157	4877.06	4878.42	1.11	0.08	SiII1193	3.08824	0.00007	4	2–21	15.79	13.36–16.08	
158	4880.58	4881.94	0.36	0.07	Lyα	3.01600	0.00030	36	8–93	13.40	13.15–13.59	α
159	4882.89	4884.26	1.20	0.10	Lyα	3.01775	0.00009	30	19–41	14.08	13.90–14.78	α
160	4885.96	4887.32	2.90	0.09	Lyα	3.01976	0.00010	30	22–40	14.75	14.38–15.64	αβ
					Lyα	3.02064	0.00008	50	32–75	14.26	14.08–14.63	αβ
161	4888.75	4890.12	1.37	0.11	Lyα	3.02242	0.00014	48	30–66	14.00	13.88–14.15	αβ
162	4898.08	4899.45	0.71	0.07	Lyα	3.03033	0.00011	17	10–30	14.11	13.76–14.84	αβγ
163	4899.95	4901.32	2.48	0.12	Lyα	3.03160	0.00014	42	30–64	14.60	14.26–15.04	αβ
164	4904.41	4905.78	0.62	0.08	Lyα	3.03546	0.00011	3	<34	16.60	13.41–16.95	αβγ
165	4906.09	4907.46	1.14	0.09	Lyα	3.03683	0.00009	36	24–46	13.96	13.82–14.20	αβγ
166	4909.91	4911.18	0.37	0.09	Lyα	3.03979	0.00025	36	4–70	13.26	12.94–14.00	αγδ
167	4917.33	4918.70	0.94	0.09	Lyα	3.04623	0.00010	35	17–52	13.85	13.71–14.20	αβγ
168	4918.86	4920.24	1.02	0.08	Lyα	3.04737	0.00008	18	12–30	14.11	13.77–14.88	αβ
169	4920.56	4921.94	0.70	0.08	Lyα	3.04877	0.00009	22	7–36	13.70	13.52–15.49	αβγ
170	4928.72	4930.09	2.54	0.12	SiIII1206	3.08571		13	5–34	15.90	13.54–16.40	)
					SiIII1206	3.08633		25	15–48	14.70	13.65–16.32	) z from SiII
171	4932.06	4933.43	2.57	0.14	SiIII1206	3.08824		36	<57	13.58	13.40–16.59	)
					Lyα	3.05873	0.00032	40	25–87	13.75	13.60–13.93	α
172	4940.99	4942.37	0.90	0.09	Lyα	3.06558	0.00007	20	13–31	13.89	13.69–14.30	αβ
173	4951.55	4952.93	1.24	0.09	Lyα	3.07436	0.00008	28	15–40	13.96	13.80–14.56	αβδ

TABLE 2—*Continued*

n	λ_{air}	λ_{vac}	EW(A)	±	ID	z	±	b (km/s)	range	logN (/cm^2)	range	Comments
174	4966.10	4967.40	20.0	:	Lyα	3.07762	0.00025	25	3–72	13.30	12.98–14.76	αβδ
					Lyα	3.07934	0.00031	32	3–82	13.28	12.92–14.20	αβ
					Lyα	3.08075	0.00010	33	24–45	14.51	14.28–14.83	αβγδ
					Lyα	3.08571				19.30	19.18–19.36	αβγδϵ)
					Lyα	3.08633				18.88	18.65–19.28	αβγδϵ) z from SiII
					Lyα	3.08824				19.40	19.32–19.49	αβγδϵ)
175	4983.15	4984.54	1.12	0.09	Lyα	3.10023	0.00011	45	35–54	13.88	13.79–13.98	αβ
176	4992.00	4993.39	1.87	0.08	Lyα	3.10740	0.00005	30	25–34	14.57	14.36–14.92	αβ
177	4993.86	4995.15	0.65	0.06	Lyα	3.10881	0.00010	45	34–56	13.80	13.70–13.89	αβ
178	5000.94	5002.34	0.58	0.07	Lyα	3.11485	0.00011	30	18–45	13.53	13.40–13.63	αβ
179	5024.28	5025.68	0.92	0.09	CIV1548	2.24626	0.00004	19	12–26	14.30	14.11–14.86	
180	5033.07	5034.47	0.88	0.11	CIV1550	2.24626	0.00004	19	12–26	14.30	14.11–14.86	
181	5048.17	5049.58	1.58	0.12	CIV1548	2.26187	0.00005	33	27–41	14.26	14.18–14.36	
182	5057.01	5058.42	0.71	0.09	CIV1550	2.26187	0.00005	33	27–41	14.26	14.18–14.36	
183	5093.19	5094.61	0.77	0.11	CIV1548	2.29086	0.00008	18	<33	13.85	13.70–17.28	
184	5101.86	5103.29	0.39	0.09	CIV1550	2.29086	or:	1	<33	17.08	13.70–17.28	
185	5148.77	5150.21	1.71	0.14	SiII1260	3.08571	0.00010	8	4–21	14.00	13.28–15.60	
					SiII1260	3.08633	0.00013	32	22–45	13.71	13.58–13.91	
186	5151.44	5152.88	0.82	0.11	SiII1260	3.08824	0.00007	4	2–21	15.79	13.36–16.08	

NOTES:—If more than one Lyman line in any redshift system would fall in the observed wavelength range, the positions of all the Lyman lines, except those badly affected by blends from lines at other redshifts, are used to determine z, b, and N. The greek letters in the Comments column indicate which Lyman lines are used in each case.

Vertical bars indicate blended features. The redshift error estimate for each component of a blend is determined by assuming that all the other components have the z, b, and N values given in the table, and we quote only the value for a shift toward the weaker neighbor. Thus, the redshift error may be an underestimate, particularly for weak features in the wings of strong lines.

Continuum-fitting errors have not been included in the analysis. Trials with different continuum estimates suggest that the additional uncertainty in the equivalent widths is usually about 0.02 Å.

[a] Determination of z, b, and N significantly affected by Lyman lines from higher redshift systems.

$\langle b \rangle = 26.9 \pm 1.7$ determined at redshift $z_{abs} \approx 2$ by Carswell *et al.* (1984). However, such a comparison may not be appropriate since the detection limit in the two cases is rather different. If we restrict consideration to systems for which $\log [N(\text{H I})] > 13.75$ (rather than the 14.0 used above, so as to retain an adequate sample size at redshift $z_{abs} = 2$), then $\langle b \rangle = 30.1 \pm 2.5$ at $z_{abs} = 2.0$ and $\langle b \rangle = 34.4 \pm 1.6$ at $z_{abs} = 2.9$. Thus there is no evidence that the velocity dispersion changes with redshift, at least over the range $z_{abs} \approx 2.0$ to $z_{abs} \approx 2.9$.

In considering the distribution of velocity dispersion and H I column density, we should be aware of the limitations imposed by the available data. Where lines occur in blends the b and N parameters are necessarily less certain, and we are more likely to underestimate the number of clouds involved, than if we are dealing with apparently single features. Another possible consequence is that for blended lines the relative number of systems with large velocity dispersions and high column densities will be overestimated. This trend is apparent from Figure 2, where the distributions of the best estimates for the b and N values are shown for different classes of Lyα lines which are subject to different sources of uncertainty. In particular, the velocity dispersions and column densities determined from Lyα plus at least one other line show a marked separation between those determined from components of blends and those from apparently single features. For the multiple component set $\langle b \rangle = 36.5 \pm 1.9$ km s^{-1}, and $\langle \log N \rangle = 14.29 \pm 0.09$, while for the individual lines $\langle b \rangle = 30.5 \pm 2.0$ km s^{-1} and $\langle \log N \rangle = 13.92 \pm 0.07$. We cannot say if the whole of the

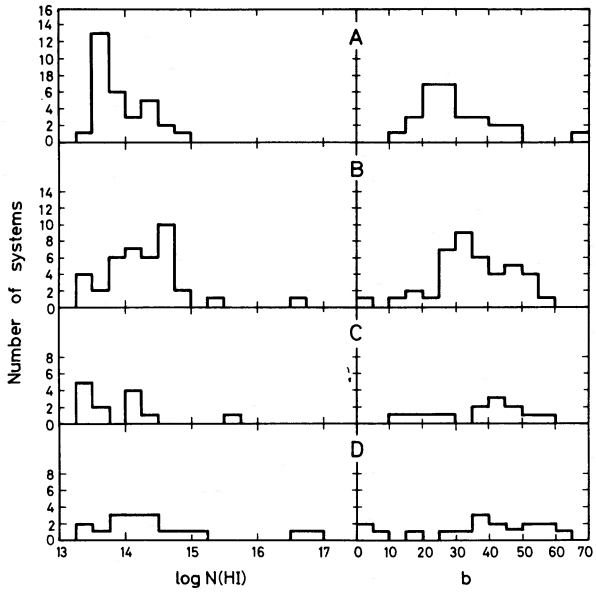

FIG. 2.—The H I column-density and velocity-dispersion distributions for Lyman line systems with $z_{abs} > 2.72$. The categories used are as follows: (*A*) Lyα not blended, and at least one other Lyman line not badly blended; (*B*) Lyα blended, and at least one other Lyman line position usable; (*C*) Lyα not blended, and no other Lyman line position usable; (*D*) Lyα and all other Lyman lines blended.

difference is due to inadequacies in the data and its analysis, but if we assume that the lines we have treated as being single do represent the true population distribution, then, for log N(H I) > 13.75, we find $\beta = 2.03 \pm 0.25$. For comparison, the Carswell *et al.* (1984) data on Q1101−264 gives $\beta = 2.20 \pm 0.33$ for log N(H I) > 13.0. Thus, while there are uncertainties in the forms of the velocity-dispersion and H I column-density distributions, where comparisons are made between quantities derived in similar ways there is no evidence for differences in the shape for either distribution over the redshift range $z \approx 2$ to $z \approx 3$.

If the lines are nearly optically thin, then a system which is found to have a high velocity dispersion through counting two (or more) lines as one will also have an unusually high H I column density. As a result we might expect to find a spurious correlation between the velocity dispersion and column density when we examine the overall sample. None was found in our data, though the large errors in b and N for low-velocity-dispersion systems with log $N > 14$ could well mask such an effect. However, this effect may well provide an explanation for the possible correlation noted by Carswell *et al.* (1984) from their data on Q1101−264.

The evolution of line numbers with redshift may be reexamined in terms of a fixed limiting H I column density rather than a Lyα equivalent width. For all systems with $2.72 < z_{abs} < 3.08$ in Q0420−388, and derived log $N > 13.75$ for the combined material from Carswell *et al.* (1984) and here, we find $\gamma = 2.1 \pm 0.9$. This is a little higher than the equivalent-width-limited result, but not significantly so.

We turn briefly to the question of heavy-element abundances in the Lyman-line–absorbing clouds. Norris, Hartwick, and Peterson (1983) have found, by summing the spectra of many different clouds reduced to rest, that there is evidence for O VI absorption being present. They infer that, typically, log (O VI/H I) ≈ −1.1, and so the abundance [O/H] ≈ −1.8. However, Sargent and Boksenberg (1983) report on a similar analysis in which no O VI was detected, so the question of abundances in these clouds remains open. The results of our search for O VI at the redshifts of the highest reliable H I column density systems in Q0420−388 are given in Table 3. In no case is the O VI doublet seen, and if we assume that the O VI and H I share the same velocity dispersion, then log (O VI/H I) < −0.7. If the clouds are in ionization balance under the radiation field used in § III*b*, then for $z = 2.8$ and number density $n < 10^{-2}$ atoms cm^{-3}, we find [O/H] < −1.8. Our less stringent O VI/H I upper limit is offset by our use of a higher ionizing flux than Norris *et al.*, to give, coincidentally, a limit in our case equal to their best estimate. If we suppose that the line widths are thermal, then the velocity dispersion appropriate for O VI is one-quarter that for H I. Under these circumstances the abundance limits are higher and not very useful.

TABLE 3

HIGH H I COLUMN DENSITY SYSTEMS

z	log N(H I)	b	log N(O VI)	log N(O VI)[a]
2.93607	15.00	40	<14.58	<17.45
2.95132	15.41	48	blend	blend
2.96177	14.75	33	<14.35	<16.35
2.98800	14.78	21	<14.00	<14.30
3.01227	14.70	48	<14.25	<14.40
3.01976	14.75	30	<14.05	<14.25

[a] Adopted b parameter is $\frac{1}{4}$ that for H I.

Summing many of the systems does not help us much, since the result is then dominated by clouds with low H I column densities, and we are unable to determine the O VI limit using an unambiguous velocity dispersion.

Searches for deuterium in Lyman line systems have been described by Atwood, Baldwin, and Carswell (1983) using the spectra presented here, and also by Chaffee *et al.* (1983) and Carswell *et al.* (1984). As is evident from Table 3, there are no systems in Q0420−388 with reliable H I column densities much above 10^{15} cm^{-2}, and so if deuterium were to be detected the observed D/H ratio would have to be 10^{-2} or more. Since plausible cosmological models give D/H < 10^{-4} (Pagel 1982), we are unable to provide an interesting upper limit.

b) Comparison with Models

The small or zero change in velocity dispersion with redshift which we find here is consistent with the models described by Ostriker and Ikeuchi (1983), in which the clouds expand isothermally in pressure balance with an adiabatically expanding intergalactic medium (IGM). However, the details of the cloud expansion will generally depend on the density. At low densities they will expand (and cool) adiabatically, since the heating and cooling time scales are long compared with the local Hubble time. On the other hand, at high densities they will expand and perhaps even increase in temperature as they try to maintain thermal equilibrium with the background ionizing radiation from quasars. Note that, in the absence of turbulent pressure, if ionization and thermal equilibrium with the background radiation apply, then all clouds at a given redshift necessarily have the same temperatures and densities, since they must simultaneously satisfy the pressure constraint (see Carswell *et al.* 1984). The range of velocity dispersions observed must then arise from turbulence within the clouds, and the minimum value will be the best estimator for the true temperature.

Following Ostriker and Ikeuchi (1983), we have computed the time (and hence redshift) evolution of some model clouds, assuming that they consist entirely of hydrogen and helium, are in pressure balance with an adiabatically expanding hot intergalactic medium at closure density corresponding to $H_0 = 50$ km s^{-1} Mpc^{-1}, and are exposed to power law radiation ($f_\nu \propto \nu^{-\alpha}$, $\alpha = 0.75$) from quasars following the Schmidt and Green (1983) distribution law for high quasar surface densities (their model HH5). We have not required that the clouds be in ionization or thermal equilibrium with the background flux, but rather have used a full time-dependent code. Calculations of the integrated background flux from any class of objects are described by McVittie (1965). We have performed a similar calculation for a $q_0 = \frac{1}{2}$ model universe, modifying his equations to take account of the Schmidt and Green form of the evolution of the ionizing flux. The maximum and minimum quasar luminosities were simply chosen to be the maximum and minimum values for which Schmidt and Green quote their density function. The resultant flux at the Lyman limit is shown as a function of redshift in Figure 3. The rates for ionization, recombination, heating, and cooling were taken from a compilation by Black (1981).

Sherman (1982) has given a possible range of present temperatures for the intergalactic medium (IGM) at critical density, $1.6 \times 10^5 < T_{IGM}{}^0 < 4.2 \times 10^6$ K; we have made the (fairly arbitrary) choice of $T_{IGM}{}^0 = 3 \times 10^5$ K. Then, for example, if the cloud is in equilibrium at redshift $z = 3$, the

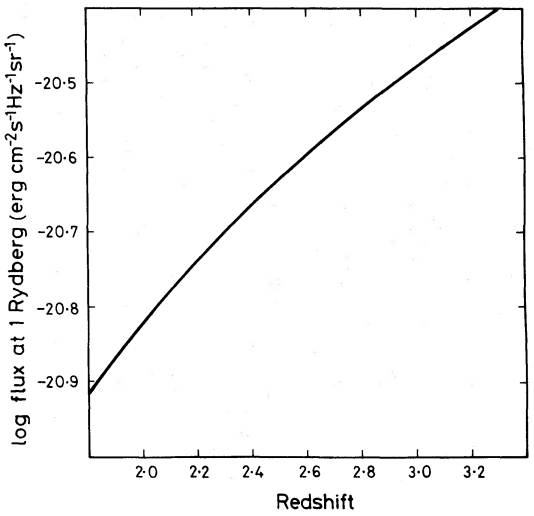

FIG. 3.—The integrated quasar background flux at the Lyman limit as seen by an observer at redshift z. See text for details.

density is then 2.9×10^{-2} atoms cm^{-3}, and the temperature 2.5×10^4 K. At $z = 2$ we find that the density falls to 5.6×10^{-3} atoms cm^{-3} and the temperature rises to 2.9×10^4 K. The neutral hydrogen fraction evolves from 6.0×10^{-4} to 2.3×10^{-4}, so the H I column density in an isotropically expanding cloud would decrease by a factor of 7.8. The temperature change corresponds to a change in velocity dispersion from 20 km s^{-1} at $z = 3$ to 22 km s^{-1} at $z = 2$, which is too small to be detected.

Lower density clouds expand more nearly adiabatically, but have very high temperatures if pressure balance is to be maintained. If we set our initial conditions arbitrarily at $z = 3.2$, for example, then we find that for an initial density greater than 3×10^{-3} atoms cm^{-3} the cloud conditions relax to the near-equilibrium solution given above, and for densities less than 1×10^{-3} atoms cm^{-3} the clouds expand and cool approximately adiabatically. In this latter case the temperatures invariably exceed 10^5 K, and this is too high a value given the measured H I velocity dispersions.

A further important point concerns the sizes of the clouds. Lower limits to individual cloud sizes have been determined by Weymann and Foltz (1983) and Foltz *et al.* (1984), using spectra of the images of gravitationally lensed quasars. For lines with rest frame equivalent width ≈ 0.5 Å at redshift $z = 2$, the Foltz *et al.* lower limit to the cloud size is of order 5–25 kpc. If we choose an H I column density of 10^{15} cm^{-2}, a value suggested by the equivalent widths of the lines observed by Foltz *et al.*, the predicted path length through a uniform cloud at $z = 2$ on our chosen model is 300 pc. This is much smaller than the Foltz *et al.* observations allow.

The cloud density, temperature, and size estimates are critically dependent on the assumed pressure for the confining IGM. If we suppose, for example, that the IGM density is 1/10 the critical value and, as before, $T_{IGM}{}^0 = 3 \times 10^5$ K, then the cloud densities are lower, their temperatures higher, and the inferred sizes greater near equilibrium at any redshift. Figure 4 shows the dependence on redshift of the temperature and density under these assumptions. It is found that clouds near or above the local equilibrium density at redshifts above $z \approx 3$ quickly relax toward the equilibrium conditions, while lower density clouds expand with close to adiabatic behavior. The estimated size of a cloud with H I column density 10^{15} cm^{-2} at $z = 2$ is now 125 kpc, and so is consistent with the observed limit. Since there are no gross inconsistencies with observed quantities, we use the model with IGM density 0.1 times the critical density, and present day temperature $T_{IGM}{}^0 = 3 \times 10^5$ K, to illustrate points made in the discussion below. Numerical details will be altered by a different choice of the IGM pressure, but many of the general trends remain the same.

We wish to relate the observed H I column density distribution function with the distribution of some intrinsic property, such as the masses of the clouds, which we suppose do not change with redshift. For a $q_0 = \frac{1}{2}$ universe with a uniform comoving population of clouds, the cloud density function for redshift z and mass m is given by

$$dn(m, z) = n_0 4\pi \left(\frac{c}{H_0}\right)^3 A(z)^2 \frac{dz}{(1+z)^{7/2}} f(m)dm \,. \quad (1)$$

Here n_0 is the local cloud density, $f(m)$ is the unknown mass distribution function, and $A(z) = 2[(1+z) - (1+z)^{1/2}]$. If the size of a cloud of mass m at redshift z is y, then, from the standard angular diameter versus redshift relation, the probability that a given cloud will intersect a given line of sight is

$$p = \frac{1}{4\pi}\left[\frac{y(1+z)}{(c/H_0)A(z)}\right]^2 . \quad (2)$$

Combining (1) and (2), we find that the number of clouds intersecting the line of sight is, on average,

$$dn_i(m, z) = n_0 \frac{c}{H_0} y^2 \frac{dz}{(1+z)^{3/2}} f(m)dm \,. \quad (3)$$

If we suppose that, for a cloud of mass m at some redshift z, the path length through the cloud is y (so ignoring any geometrical effects), then the observed H I column density N is

$$N = Xny \,, \quad (4)$$

where X is the neutral hydrogen fraction and n the total hydrogen number density. The mass m may be measured in units such that

$$m = ny^3 \,. \quad (5)$$

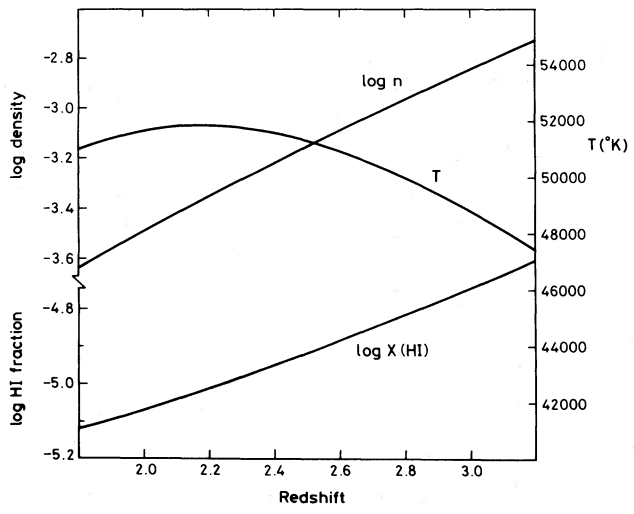

FIG. 4.—The redshift dependence of the temperature, density, and hydrogen ionization fraction in a pressure-confined cloud in the IGM (see text).

Hence the number of clouds of mass m intersecting the line of sight to a quasar is given by

$$dn_i(m, z) = n_0 \frac{c}{H_0} \frac{dz}{(1+z)^{3/2}} n^{-2/3} m^{2/3} f(m) dm . \quad (6)$$

The observed column-density distribution function along a line of sight has the form

$$dn_i(z, N) = h(z) dz N^{-\beta} dN , \quad (7)$$

where β is, to a reasonable approximation, independent of the redshift. Since $N = Xny = Xn^{2/3}m^{1/3}$, we have

$$dn_i(z, N) = \frac{h(z)}{3} dz X n^{2/3} m^{-2/3} (X n^{2/3} m^{1/3})^{-\beta} dm . \quad (8)$$

From the models for cloud evolution we find that X and n are independent of m and are functions only of the redshift z. This allows us to compare equations (6) and (8) to determine that

$$f(m) = K m^{-(\beta+4)/3} , \quad (9)$$

where K is some constant. Thus, if we choose $\beta = 1.75$, the weighted mean value from Carswell *et al.* (1984) and this paper $f(m) = Km^{-1.92}$. The number of clouds of mass m intersecting the line of sight at redshift z is then

$$dn_i(m, z) = n_0 K \frac{c}{H_0} \frac{dz}{(1+z)^{3/2}} n^{-2/3} m^{-(\beta+2)/3} dm . \quad (10)$$

For a cloud to be observed we require that the H I column density exceed some value $N_0 = Xn^{2/3}m_0{}^{1/3}$. The total number of clouds observable per unit redshift is then obtained by integrating equation (10) over m with lower limit m_0. This yields

$$\frac{dN_i(z, >N_0)}{dz} = n_0 K \frac{c}{H_0} \frac{3}{\beta - 1} \frac{1}{N_0{}^{\beta-1}} \frac{X^{\beta-1} n^{2(\beta-2)/3}}{(1+z)^{3/2}} . \quad (11)$$

Since we may compute $X(z)$ and $n(z)$, knowledge of the exponent β allows us to predict the form of the redshift dependence of the number of systems. Blending of lines will affect the redshift dependence, but we have not attempted to allow for it here. A similar expression has been presented by Ostriker and Ikeuchi (1983). We have derived it here to retain the hydrogen ionization fraction and the density explicitly. Note that our parameter β is not the same as that used by Ostriker and Ikeuchi.

The predicted cloud numbers depend critically on the value of β. In Figure 5 we illustrate, using the standard model, the behavior of cloud numbers with redshift for a range of values of β including the average observed value $\beta = 1.75$. In comparing these theoretical curves with the observations, it is as well to recall that we have been able to determine the redshift dependence only for $2 < z < 3$, or $0.48 < \log(1+z) < 0.6$, so a power-law fit to the data is an adequate approximation.

Evidently, the value $\beta = 1.75$ determined earlier using all the absorption-line measurements gives an unacceptable value for the power law exponent in the fit to the number of systems. Agreement comes only for β a little above 2, consistent with the mean value of $\beta = 2.09 \pm 0.20$ obtained from the apparently unblended Lyα lines in the Q0420−388 and Q1101−264 spectra. If a lower IGM pressure is allowed, then the required value for β falls a little, but is still close to 2. A longer redshift baseline and improved estimates of the H I column density distribution function would allow a more stringent test of the model.

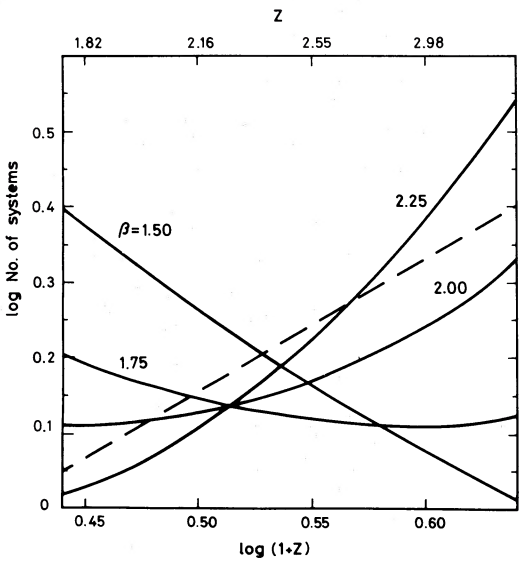

FIG. 5.—The predicted dependence of the observed cloud numbers on the redshift for a range of observed H I column-density distribution functions of the form $N^{-\beta}dN$. Curves are marked with the relevant values of β, and the observed $(1+z)^2$ cloud number dependence is shown as a dashed line for comparison.

The same general considerations will apply for adiabatically expanding clouds, since the ionization and density then depend on the initial values, and not on the cloud masses. The precise redshift dependence of the number of systems then depends on the mix of parameters at some epoch, but it is of value to examine this for a few cases. We find that for low-density systems ionization balance is achieved before thermal balance, and as the clouds expand and cool in a decreasing background flux, the hydrogen tends to recombine. As a result more clouds become detectable as the redshift decreases, and, if β is positive then γ must be negative. Thus, if the model is correct, the clouds we observe cannot be expanding adiabatically.

The assumption we have used that the cloud mass does not change significantly with redshift requires that evaporation from the clouds is not important. Cowie and McKee (1977) give an expression for the characteristic time for evaporation which, applied to our illustrative model, gives timescales $t_{evap} \approx 3 \times 10^{-20} N^2$ yr at $z = 2$ and $t_{evap} \approx 4 \times 10^{-22} N^2$ yr at $z = 3$. For $N = 10^{14}$ cm^{-2}, the classical evaporation times are 3×10^8 yr at $z = 2$ and 4×10^6 yr at $z = 3$, i.e., somewhat shorter than the Hubble times at these redshifts. A consequence of evaporation at these rates is that low–column-density clouds would effectively disappear and high–column-density systems remain largely intact. This would lead to large differences in the numbers of clouds at different redshifts, and, contrary to the results inferred from the observations, large differences in the shape of the column-density distribution function at different redshifts. However, this conflict does not necessarily imply that the intergalactic cloud picture is incorrect, since even very small magnetic fields (10^{-12} G is sufficient) effectively reduce the thermal conductivity and so inhibit evaporation (Spitzer 1962). We note that for the gas around M87 Binney and Cowie (1981) find that the effective thermal conductivity is less than about 2.10^{-3} of the classical value (Spitzer, 1962) used above.

We have considered the pressure—confined gas cloud model because it is the one suggested by Sargent *et al.* (1980) as a

result of their investigation of Lyman-line systems and because the consequences of such a model may easily be compared with observations. However, other, rather different pictures are not excluded. One obvious possibility is that the clouds are at least partly gravitationally bound, so pressure confinement does not play a dominant role. Models based on this have been considered by Black (1981). Self-gravity from the gas cloud itself should lead to a velocity-dispersion–column-density correlation, though it is not clear how strong such a correlation should be. Also, it is difficult at this stage to be sure that any such correlation is not a result of difficulties in determining the velocity dispersion and column density from noisy line profiles, as discussed in § III*a*.

The absence of any clustering on velocity scales of greater than 300 km s^{-1} implies that most of the clouds are not associated with clusters of galaxies (Sargent *et al.* 1980), but the evidence that they are not associated with single-field or dwarf galaxies is weak. It is difficult to examine the two point-correlation function on scales less than about 70 km s^{-1} because then the separations become comparable to the line widths. There is no significant evidence for clustering on scales greater than this in the Q0420−388 spectrum, but some suggestion of a peak in the two-point correlation function on scales up to about 150 km s^{-1}. Similar behavior was found in the Q1101−264 spectra by Carswell *et al.* (1984).

IV. SUMMARY

The Lyman absorption lines are almost invariably resolved at 15 km s^{-1} (FWHM) resolution, and most are resolved at the 33 km s^{-1} resolution we have used to study the spectrum of Q0420−388. The velocity dispersion and H I column density in each absorbing cloud have therefore been determined by fitting Voigt profiles to all the available Lyman lines. A difference in the velocity-dispersion and column-density distributions between the Lyα lines which are apparently single and those where the lines are blended is possibly due to our having insufficient S/N to adequately separate the components of the blend. A possible result of this is that there may be an apparent (weak) correlation between column density and velocity dispersion. Our data show none, but such an effect may provide an explanation of the possible correlation noted by Carswell *et al.* (1984). This uncertainty also affects estimates of the clustering of the Lyman systems, in that if they all have the same properties statistically, then they could be clustered on scales comparable to the line widths. This point required further investigation.

Where we have reason to believe that we are comparing quantities which are affected in the same way by blending uncertainties, we have found no evidence for redshift dependence over the range $z = 2$ to $z = 3$ of the distribution functions for the internal velocity dispersions in the clouds (and so, possibly, their temperatures), or for the observed H I column densities, apart from a scaling factor which reflects the change of cloud numbers with redshift. The H I column density distribution is well approximated by a power law with index very roughly equal to 2.

In principle we may use the H I column-density distribution power law to predict the redshift dependence of the number of clouds if we have a model for how individual clouds evolve with redshift. We have considered the case in which there is a uniform comoving population of clouds which are ionized and heated by the integrated QSO background flux and pressure confined by an adiabatically expanding IGM. We then find that the uncertainty in the H I column-density distribution function (which is largely due to unquantified selection effects) allows a wide range of possibilities for the redshift dependence in the number of clouds we will see, and is consistent with the observed $(1 + z)^2$ redshift dependence. Another possible model, in which the clouds expand adiabatically following the expansion of the universe, is ruled out.

We have found no systems in which the cosmologically important deuterium-to-hydrogen ratio could be measured. Generally, if D/H $\approx 10^{-4}$ or less, and the detection limit is of order 10^{13} cm^{-2}, H I column densities in excess of 10^{17} cm^{-2} would be required. These are rare.

We thank the mountain staff at CTIO and the AAT for their assistance with the observations. R. F. C. acknowledges support from the Radcliffe Trust and the UK Science and Engineering Research Council, and the SERC for provision of computing facilities through Starlink.

REFERENCES

Atwood, B., Ingerson, T., Lasker, B. M., and Osmer, P. S. 1979, *Pub. A.S.P.*, **91**, 120.
Atwood, B., Baldwin, J. A., and Carswell, R. F. 1982, *Ap. J.*, **257**, 559.
———. 1983, *Proc. 24th Liège Internat. Colloquium, Quasars and Gravitational Lenses*, ed. J. P. Swings (Université de Liège, Inst. d'Astrophysique) p. 581.
Black, J. H. 1981, *M.N.R.A.S.*, **197**, 553.
Binney, J., and Cowie, L. L. 1981, *Ap. J.*, **247**, 464.
Carswell, R. F., Whelan, J. A. J., Smith, M. G., Boksenberg, A., and Tytler, D. 1982, *M.N.R.A.S.*, **198**, 91.
Carswell, R. F., Morton, D. C., Smith, M. G., Stockton, A. N., Turnshek, D. A., and Weymann, R. J. 1984, *Ap. J.*, **278**, 486.
Chaffee, F. H., Weymann, R. J., Latham, D. W., and Strittmatter, P. A. 1983, *Ap. J.*, **267**, 12.
Chaffee, F. H., Foltz, C. B., Röser, H.-J., Weymann, R. J., and Latham, D. W. 1984, *Ap. J.*, submitted.
Cowie, L. L., and McKee, C. F. 1977, *Ap.J.*, **211**, 135.
Foltz, C. B., Weymann, R. J., Roser, H. J., and Chaffee, F. H. 1984, *Ap. J. (Letters)*, **281**, L1.
McVittie, G. C. 1965, *General Relativity and Cosmology* (Urbana: University of Illinois Press).
Norris, J., Hartwick, F. D. A., and Peterson, B. A. 1983, *Ap. J.*, **273**, 450.
Osmer, P. S., and Smith, M. G. 1976, *Ap. J.*, **210**, 267.
Ostriker, J. P., and Ikeuchi, S. 1983, *Ap. J. (Letters)*, **268**, L63.
Pagel, B. E. J. 1982, *Phil. Trans. Roy. Soc. London, A*, **307**, 19.
Peterson, B. A. 1978, *IAU Symp. 79, The Large Scale Structure of the Universe*, ed. M. S. Longair and J. Einasto (Dordrecht: Reidel), p. 389.
———. 1983, *Proc. 24th Liège Internat. Colloquium, Quasars and Gravitational Lenses*, ed. J. P. Swings (Université de Liège, Inst. d'Astrophysique), p. 563.
Sargent, W. L. W., and Boksenberg, A. 1983, *Proc. 24th Liège Internat. Colloquium, Quasars and Gravitational Lenses*, ed. J. P. Swings (Université de Liège, Inst. d'Astrophysique), p. 518.
Sargent, W. L. W., Young, P. J., Boksenberg, A., and Tytler, D. 1980, *Ap. J. Suppl.*, **42**, 41.
Schmidt, M., and Green, R. F. 1983, *Ap. J.*, **269**, 352.
Sherman, R. D., 1982. *Ap. J.*, **256**, 370.
Smith, M. G. 1976, *Ap. J. (Letters)*, **206**, L125.
Smith, M. G., *et al.* 1981, *M.N.R.A.S.*, **195**, 437.
Spitzer, L. 1962, *Physics of Fully Ionized Gases* (New York: Interscience).
Weymann, R. J., and Foltz, C. B. 1983, *Ap. J. (Letters)*, **272**, L1.
Young, P. J., Sargent, W. L. W., and Boksenberg, A. 1982, *Ap. J.*, **252**, 10.

B. Atwood and J. A. Baldwin: Cerro Tololo Inter-American Observatory, Casilla 603, La Serena, Chile

R. F. Carswell: Institute of Astronomy, Madingley Road, Cambridge CB3 0HA, England